Available online at www.sciencedirect.com
SCIENCE DIRECT®
Journal of Sound and Vibration 291 (2006) 627–643
JOURNAL OF SOUND AND VIBRATION
www.elsevier.com/locate/jsvi

An exact solution for free torsional vibration of a uniform circular shaft carrying multiple concentrated elements

Der-Wei Chen*

Department of Naval Architecture and Marine Engineering, Chung Cheng Institute of Technology, National Defense University, Yuansulin, Dashi, Taoyuan, Taiwan 335, ROC

Received 4 November 2004; received in revised form 16 June 2005; accepted 23 June 2005
Available online 19 August 2005

Abstract

For a uniform circular shaft carrying multiple concentrated elements (such as rotary inertias and/or torsional springs) with arbitrary magnitudes and locations, a lot of existing techniques may be used to obtain its ''approximate'' natural frequencies and mode shapes, but this is not true for the ''exact'' solutions. The purpose of this paper is to present some information in this aspect. Because the classical analytical method is lengthy and tedious for the title problem if the total number of the attached concentrated elements is larger, this paper adopts the numerical assembly method (NAM) to tackle the problem. In which, the ''left'' side and the ''right'' side of each attaching point together with the ''left'' end and the ''right'' end of a uniform circular shaft are considered as the nodal points, the associated integration constants are considered as nodal displacements and each of the associated coefficient matrices is considered as the element stiffness matrix of a shaft element, then the assembly technique of the direct stiffness matrix method for the conventional finite element method (FEM) is used to obtain the ''overall'' coefficient matrix $[B]$. Any trial value of ω_j that renders the value of the determinant $|B|$ vanishes denoting one of the eigenvalues of the uniform circular shaft carrying multiple concentrated elements, and the substitution of the associated integration constants into the relevant eigenfunctions determines the corresponding mode shape.

*Corresponding author. Tel.: +886 33 800958; fax: +886 33 892134.
E-mail address: dwchen@ccit.edu.tw.

0022-460X/$ - see front matter
doi:10.1016/j.jsv.2005.06.034

To confirm the reliability of the presented algorithm, all the numerical results obtained from the NAM were compared with the corresponding ones obtained from the published literature or the FEM and good agreement was achieved.

1. Introduction

In earlier years, the torsional vibration problem was solved using the Holzer method [1–6]. After the advent of computers, the last problem was tackled by the more effective transfer matrix method and the finite element method (FEM) [7–9]. The natural frequencies and mode shapes obtained from the above-mentioned methods are the "approximate" ones, until 1975 (and 1979), Gorman [10] (and Blevins [11]) presented the "exact" expressions for the torsional frequencies and mode shapes of a "uniform" shaft carrying a single rotary inertia (or/and torsional spring) with various non-classical boundary conditions. Ref. [12] discussed the "exact" solutions for the torsional frequencies and mode shapes of the generally constrained shafts and piping. As for the "exact" solutions of the torsional vibration of uniform shafts carrying multiple concentrated elements at arbitrary locations, the information concerned is rare and this is one of the reasons why the problem in this aspect is studied. In this paper, the numerical assembly method (NAM) [13–15] was used to perform the torsional vibration analysis of a "uniform" circular shaft carrying multiple concentrated elements (rotary inertias or/and torsional springs) with arbitrary magnitudes and locations.

From the following sections of this paper, one finds that the eigen equation of the title problem takes the form $[\mathrm{B}]\{\bar{C}\} = \{0\}$. Since the order of the overall coefficient matrix $[B]$ is $p = 2n + 2$, with n being the total number of concentrated attachments, the order of $[B]$ is 4 for one attachment, 6 for two attachments, …, and $2n + 2$ for n attachments. It is evident that the explicit expression for the eigen equation $[\mathrm{B}]\{\bar{C}\} = \{0\}$ will become lengthy and complicated for the cases with larger n, hence the literature relating to the exact solution for the torsional natural frequencies of a uniform circular shaft carrying more than "two" concentrated attachments is rare. Because the NAM presented in Refs. [14,15] was found to easily tackle the free "bending" vibration problem of the "uniform" and "non-uniform" beams carrying any number of concentrated attachments, this paper tries to use the same approach to determine the exact natural frequencies of the uniform circular shafts carrying multiple concentrated elements. The key point of the NAM is as follows: If the "left" side and the "right" side of each attaching point together with the "left" end and the "right" end of the uniform circular shaft are considered as the nodal points, and the associated integration constants, C_{vi} ($v = 1-n$; $i = 1-2$), are considered as nodal displacements, then the associated coefficient matrix, $[B_L]$, $[B_v]$ ($v = 1$–n) or $[B_R]$, may be considered as the element stiffness matrix of a shaft element, so that the conventional assembly technique of the direct stiffness matrix method for the FEM [16] may be used to obtain the "overall" coefficient matrix $[B]$. Any trial value of ω_j that renders the value of the determinant $|B|$ vanishes denoting one of the eigenvalues of the uniform circular shaft carrying multiple concentrated elements.

To show the reliability of the introduced approach, the lowest five natural frequencies and some of the corresponding mode shapes of twisting angles of a uniform circular shaft carrying five

concentrated elements were calculated. Two boundary conditions were studied: clamped–free and clamped–clamped. It has been found that the agreement between the present results and the FEM results is good.

2. Theoretical analysis of the problem

In this section, the coefficient matrices for the associated integration constants are derived and the technique for arriving at the overall coefficient matrix is introduced. The last matrices and technique are the key points for the NAM adopted in this paper.

2.1. Eigenfunctions of the constrained uniform circular shaft

Fig. 1 shows a cantilevered circular shaft carrying n concentrated elements. The whole cantilevered circular shaft with length L is subdivided into $(n+1)$ segments by the attaching point v located at $x = x_v$ $(v = 1,2,\ldots,n)$, where (v) denotes the vth "attaching point" and (v) denotes the vth "shaft segment". In addition, the "left" end and the "right" end of the shaft are denoted by Ⓛ and Ⓡ, respectively.

The equation of motion for a torsional uniform circular shaft is given by [10,12]

$$GI_p \frac{\partial^2 \theta(x,t)}{\partial x^2} - \bar{J}_p \frac{\partial^2 \theta(x,t)}{\partial t^2} = T(x,t), \tag{1}$$

where G is the shear modulus of shaft material, I_p is the (polar) moment of inertia of the cross-sectional area about the rotational (x) axis, $\bar{J}_p$ is the mass moment of inertia about the rotational (x) axis per unit length, $T(x,t)$ and $\theta(x,t)$ are, respectively, the torsional moment and the corresponding twisting angle at position x and time t. For a circular shaft of diameter d one has $I_p = \pi d^4/32$.

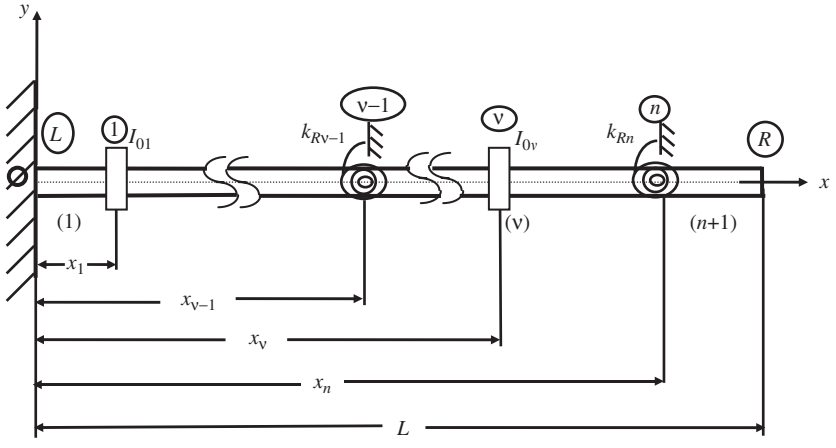

Fig. 1. A cantilevered circular shaft carrying n concentrated elements.

For free vibration of the shaft, one has

$$\theta(x,t) = \bar{\theta}(x)e^{i\omega t}, \tag{2}$$

where $\bar{\theta}(x)$ is the amplitude of twisting angle $\theta(x,t)$ and ω is the circular frequency of the torsional shaft.

Substituting of Eq. (2) into Eq. (1) and setting $T(x,t) = 0$ will lead to

$$\frac{d^2\bar{\theta}(x)}{dx^2} + \frac{\bar{J}_p\omega^2}{GI_p}\bar{\theta}(x) = 0 \tag{3a}$$

or

$$\frac{d^2\bar{\theta}(x)}{dx^2} + \beta^2\bar{\theta}(x) = 0, \tag{3b}$$

where

$$\beta^2 = \frac{\bar{J}_p\omega^2}{GI_p} \tag{4a}$$

or

$$\omega = (\beta L)\sqrt{\frac{GI_p}{\bar{J}_pL^2}}. \tag{4b}$$

The general solution of Eq. (3b) takes the form

$$\bar{\theta}(x) = C_1 \sin \beta x + C_2 \cos \beta x. \tag{5}$$

If the following non-dimensional parameter is introduced

$$\xi = x/L, \tag{6}$$

then Eq. (5) becomes

$$\bar{\theta}(\xi) = C_1 \sin \beta\xi + C_2 \cos \beta\xi, \tag{7}$$

where C_i $(i = 1–2)$ are the integration constants.

Eq. (7) represents the eigenfunction for the twisting angle of the shaft. Once the natural frequencies ω_j $(j = 1,2,\ldots)$ and the constants, C_i $(i = 1–2)$, are determined from the next sections, one may obtain the value of $\bar{\theta}_j(\xi)$. The latter are the mode shapes of the shaft corresponding to the natural frequency ω_j.

For "the vth shaft segment", from Eq. (7) one has

$$\bar{\theta}_v(\xi_v) = C_{v1} \sin(\beta\xi_v) + C_{v2} \cos(\beta\xi_v) \tag{8}$$

with

$$\xi_v = x_v/L. \tag{9}$$

2.2. Coefficient matrix $[B_v]$ for the vth attaching point

Compatibility for the twisting angles and twisting moments at the attaching point requires that

$$\bar{\theta}_v^L(\xi_v) = \bar{\theta}_v^R(\xi_v), \tag{10}$$

$$\frac{\mathrm{d}\bar{\theta}_v^L(\xi_v)}{\mathrm{d}\xi} - \frac{\beta^2}{I_{0v}^*}\bar{\theta}_v^L(\xi_v) + k_{Rv}^*\bar{\theta}_v^L(\xi_v) = \frac{\mathrm{d}\bar{\theta}_v^R(\xi_v)}{\mathrm{d}\xi} \tag{11}$$

with

$$k_{Rv}^* = \frac{k_{Rv}L}{GI_p}, \tag{12}$$

$$I_{0v}^* = \frac{\bar{J}_p L}{I_{0v}}, \tag{13}$$

where k_{Rv} and I_{0v} represent the vth set rigidly attached torsional spring constant and rotary inertia.

The substitution of Eqs. (8) and (9) in Eqs. (10) and (11) leads to

$$C_{v1}\ \sin(\beta\xi_v) + C_{v2}\ \cos(\beta\xi_v) - C_{v+1,1}\ \sin(\beta\xi_v) - C_{v+1,2}\ \cos(\beta\xi_v) = 0, \tag{14}$$

$$C_{v1}\left[\beta\ \cos(\beta\xi_v) - \frac{\beta^2}{I_{0v}^*}\sin(\beta\xi_v) + k_{Rv}^*\ \sin(\beta\xi_v)\right] - C_{v2}\left[\beta\ \sin(\beta\xi_v) + \frac{\beta^2}{I_{0v}^*}\cos(\beta\xi_v) - k_{Rv}^*\ \cos(\beta\xi_v)\right]$$
$$- C_{v+1,1}\ \beta\cos(\beta\xi_v) + C_{v+1,2}\beta\ \sin(\beta\xi_v) = 0. \tag{15}$$

It is noted that, in Eqs. (10) and (11), the "left side" of the vth attaching point located at $\xi = \xi_v$ belongs to the segment (v) and the "right side" belongs to the segment $(v+1)$, thus the associated coefficients are represented by $C_{v\mathrm{i}}$ and $\mathrm{C}_{v+1,i}$ $(i = 1\text{–}2)$, respectively, as may be seen from Eqs. (14)–(15).

Writing Eqs. (14)–(15) in matrix form gives

$$[B_v]\{C_v\} = \{0\}, \tag{16}$$

where

$$\{C_v\} = \left\{C_{v1}\ \ C_{v2}\ \ C_{v+1,1}\ \ C_{v+1,2}\right\} = \left\{\bar{C}_{2v-1}\ \ \bar{C}_{2v}\ \ \bar{C}_{2v+1}\ \ \bar{C}_{2v+2}\right\}, \tag{17a}$$

$$\bar{C}_{2v-1} = C_{v1},\ \ \bar{C}_{2v} = C_{v2},\ \ \bar{C}_{2v+1} = C_{v+1,1}\ \ \bar{C}_{2v+2} = C_{v+1,2} \tag{17b}$$

and

$$[B_v] = \begin{array}{c} \\ \\ 2v \\ 2v+1 \end{array}\begin{array}{c} \begin{array}{cccc} 2v\text{-}1 & 2v & 2v+1 & 2v+2 \end{array} \\ \begin{bmatrix} \sin(\beta\xi_v) & \cos(\beta\xi_v) & -\sin(\beta\xi_v) & -\cos(\beta\xi_v) \\ \beta\ \cos(\beta\xi_v) - \frac{\beta^2}{I_{0v}^*}\ \sin(\beta\xi_v) + k_{Rv}^*\ \sin(\beta\xi_v) & -\beta\sin(\beta\xi_v) - \frac{\beta^2}{I_{0v}^*}\cos(\beta\xi_v) + k_{Rv}^*\ \sin(\beta\xi_v) & -\beta\ \cos(\beta\xi_v) & \beta\ \sin(\beta\xi_v) \end{bmatrix} \end{array}. \tag{17c}$$

2.3. Coefficient matrix $[B_L]$ for the left end of the circular shaft

For a cantilever shaft with left end clamped, the boundary condition is

$$\bar{\theta}(0) = 0. \tag{18}$$

From Fig. 1 one sees that the left end of the shaft, Ⓛ, coincides with the left end of the first shaft segment ($v = 1$), from Eqs. (8), (9) and (18) one obtains

$$C_{12} = 0. \tag{19}$$

Writing Eq. (19) in matrix form gives

$$[B_L]\{C_L\} = \{0\}, \tag{20}$$

where

$$[B_L] = \begin{matrix} 1 & 2 \\ [0 & 1]1, \end{matrix} \tag{21}$$

$$\{C_L\} = \{C_{11}\ C_{12}\} = \{\bar{C}_1\ \bar{C}_2\}, \tag{22}$$

where the [ ] and { } represent the rectangular matrix and the column vector, respectively, and

$$\bar{C}_1 = C_{11},\ \ \bar{C}_2 = C_{12}. \tag{23}$$

In Eq. (21) and the subsequent equations, the digits shown on the top side and right side of the matrix represent the identification numbers of degrees of freedom (dof) for the associated constants $\bar{C}_i$ ($i = 1,2,\ldots$).

2.4. Coefficient matrix $[B_R]$ for the right end of the circular shaft

For a cantilever shaft with right end free, the boundary condition is

$$\frac{\mathrm{d}\bar{\theta}(1)}{\mathrm{d}\xi} = 0. \tag{24}$$

Since the right end of the shaft, Ⓡ, coincides with the right end of the $(n+1)$th segment ($\nu = n+1$), as one may see from Fig. 1, from Eqs. (8), (9) and (24) one obtains

$$\beta\ \cos(\beta)C_{n+1,1} - \beta\ \sin(\beta)C_{n+1,2} = 0. \tag{25}$$

Writing Eq. (25) in matrix form gives

$$[B_R]\{C_R\} = \{0\}, \tag{26}$$

where

$$[B_R] = \begin{matrix} 2n+1 & 2n+2 \\ [\beta\ \cos(\beta) & -\beta\ \sin(\beta)]p, \end{matrix} \tag{27}$$

$$\{C_R\} = \{C_{n+1,1}\ \ C_{n+1,2}\} = \{\bar{C}_{2n+1}\ \ \bar{C}_{2n+2}\}, \tag{28}$$

$$\bar{C}_{2n+1} = C_{n+1,1}, \quad \bar{C}_{2n+2} = C_{n+1,2}, \tag{29}$$

$$p = 2n + 2. \tag{30}$$

In the last equation, p represents the total number of equations. From the above derivations one sees that from each attaching point for a concentrated element one may obtain two (compatibility) equations and from each boundary (Ⓛ or Ⓡ) one may obtain one equation. Hence, for a circular shaft carrying n concentrated elements, the total number of equations that one may obtain for the integration constants C_{vi} ($v = 1-n$, $i = 1-2$) is equal to $2n + 2$, i.e., $p = 2n + 2$ as shown by Eq. (30). Of course, the total number of unknowns (C_{vi}) is also equal to $2n + 2$. From Eq. (8) one sees that the solution $\bar{\theta}_v(\xi)$ for each shaft segment contain two unknown integration constants C_{vi} ($i = 1-2$), hence if a shaft carries n concentrated elements, then the total number of the shaft segment is $n + 1$ and thus the total number of unknown (C_{vi}) is equal to $2(n + 1) = 2n + 2 = p$.

For a cantilever shaft with its right end free, the boundary condition is

$$\bar{\theta}(1) = C_1 \sin \beta + C_2 \cos \beta = 0 \tag{31}$$

or in matrix form

$$[B_R]\{C_R\} = \{0\}, \tag{32}$$

where

$$[B_R] = \begin{matrix} 2n+1 & 2n+2 \\ [\sin \beta & \cos \beta] \end{matrix} p. \tag{33}$$

The column vector $\{C_R\}$ is the same as that given by Eq. (28).

2.5. Overall coefficient matrix [B] of the entire circular shaft and the frequency equation

If all the unknowns C_{vi} ($v = 1$–n, $i = 1$–2) are replaced by a column vector $\{\bar{C}\}$ with coefficients $\bar{C}_k$ ($k = 1,2, \ldots, p$) defined by Eqs. (17b), (23) and (29), then the matrices $[B_L]$, $[B_v]$ and $[B_R]$ are similar to the element property matrices (FEM) with corresponding identification numbers for the dof shown on the top side and right side of the matrices defined by Eqs. (17c), (21) and (27). Based on the assembly technique for the direct stiffness matrix method, it is easy to arrive at the following coefficient equation for the entire vibrating system:

$$[B]\{\bar{C}\} = \{0\}. \tag{34}$$

The non-trivial solution of the problem requires that

$$|B| = 0, \tag{35}$$

which is the frequency equation, and the half-interval technique [16] may be used to solve the non-dimensional frequency parameters β_j (j = 1,2,…) and, in turn, the natural frequencies eigenvalues ω_j. To substitute the value of β_j into Eq. (34) one may determine the values of unknowns $\bar{C}_k$ ($k = 1,2,\ldots, p$). Among which, from Eq. (17b) one sees that $\bar{C}_{2v-1} = C_{v1}$, $\bar{C}_{2v} = C_{v2}$, $\bar{C}_{2v+1} = C_{v+1,1}$, $\bar{C}_{2v+2} = C_{v+1,2}$ (v = 1–n), hence the substitution of C_{vi} ($i = 1-2$) into Eq. (8) will define the corresponding mode shape $\bar{\theta}_{(j)}(\xi)$. For a cantilever shaft carrying a ($n = 1$) set of

and two ($n = 2$) sets of concentrated elements, the corresponding overall coefficient matrices $[B]_{(1)}$ and $[B]_{(2)}$ were shown in Appendix A [see Eqs. (A.1), (A.2)]. From the lengthy expressions one sees that the conventional explicit formulations are not suitable for a shaft carrying more than two ($n > 2$) sets of concentrated elements. However this is not true for the numerical assembly method (NAM) adopted in this paper.

3. Numerical results and discussions

The dimensions and physical properties of the circular shaft studied in this paper are: shaft length $L = 40$ in, shear modulus of shaft material $G = 1.2 \times 10^7$ psi, mass density of shaft material $\rho = 0.283\,\text{lbm/in}^3$, shaft diameter $d = 1$ in. For convenience, two non-dimensional parameters for each concentrated element were introduced: $I^*_{0v} = \tilde{J}_p L/I_{0v}$ and $k^*_{Rv} = k_{Rv}L/GI_p$, $v = 1,2,\ldots,n$. In addition, the two-letter acronyms, CF and CC, were used to denote the clamped–free (CF) and clamped–clamped (CC) boundary conditions of the shaft, respectively.

3.1. Comparing with the existing literature

In order to compare the results of NAM with the corresponding ones obtained by Gorman [10], the CF and CC circular shafts without carrying any concentrated elements were studied first. The lowest five non-dimensional frequency coefficients, β_j ($j = 1$–5), were shown in Table 1. It is evident that the results of the NAM and those of Gorman [10] are in good agreement.

For the cantilever shaft carrying a single "torsional spring" located at $\xi = x/L = 1.0$ and 0.5, respectively, Table 2(a) shows the lowest five non-dimensional frequency coefficients, β_j ($j = 1$–5), obtained from the NAM and those from Gorman [10] for the non-dimensional torsional springs $k^*_{Rv} = k_{Rv}L/GI_p = 0.1$, 1.0 and 10.0, while Table 2(b) shows those for the non-dimensional rotary inertia $I^*_{0v} = \tilde{J}_p L/I_{0v} = 0.1$, 1.0 and 10.0. Similarly, for the same cantilever shaft carrying a single "rotary inertia" located at $\xi = x/L = 1.0$ and 0.5, respectively, Tables 3(a) and (b) show the similar information for the similar cases. It is also found that the values of β_j ($j = 1$–5) obtained from the NAM are very close to those of Gorman [10].

For the cantilever shaft carrying "two" concentrated elements (one rotary inertia and one torsional spring) at its free end with magnitudes of the non-dimensional torsional spring, $k^*_{Rv} =$

Table 1
The lowest five non-dimensional frequency coefficients β_j ($j = 1$–5) for the CF and CC uniform shafts without carrying any concentrated elements

Boundary conditions	Methods	Non-dimensional frequency coefficients				
		β_1	β_2	β_3	β_4	β_5
CF	NAM	1.570796	4.712389	7.853982	10.995575	14.137167
	Gorman [10]	1.570795	4.712391	7.853986	10.995571	14.137167
CC	NAM	3.141593	6.283185	9.424777	12.566370	15.707963
	Gorman [10]	3.141594	6.283188	9.424774	12.566369	15.707964

NAM = numerical assembly method.

Table 2
The lowest five non-dimensional frequency coefficients β_j ($j = 1$–5) for a cantilever shaft carrying a single "torsional spring"

$k^*_{R1} = \frac{k_{R1}L}{GI_p}$	Methods	Non-dimensional frequency coefficients				
		β_1	β_2	β_3	β_4	β_5
(a) located at $\xi_1 = x_1/L = 1.0$						
0.1	NAM	1.631994	4.733512	7.866693	11.004661	14.144237
	Gorman[10]	1.631996	4.733514	7.866691	11.004663	14.144237
1.0	NAM	2.028758	4.913181	7.978666	11.085538	14.207437
	Gorman[10]	2.028753	4.913177	7.978667	11.085534	14.207442
10.0	NAM	2.862773	5.760558	8.708313	11.702678	14.733472
	Gorman[10]	2.862776	5.760559	8.708312	11.702677	14.733469
(b) Located at $\xi_1 = x_1/L = 0.5$.						
0.1	NAM	1.601997	4.722975	7.860343	11.000122	14.140703
	Gorman[10]	1.601996	4.722977	7.860344	11.000122	14.140702
1.0	NAM	1.836597	4.815843	7.917052	11.040830	14.172433
	Gorman[10]	1.836595	4.815840	7.917054	11.040826	14.172431
10.0	NAM	2.653662	5.454353	8.391346	11.408627	14.469869
	Gorman[10]	2.653665	5.454351	8.391342	11.408627	14.469869

NAM = numerical assembly method.

Table 3
The lowest five non-dimensional frequency coefficients β_j ($j = 1$–5) for a cantilever shaft carrying a single "rotary inertia"

$I^*_{01} = \frac{\bar{J}_p L}{I_{01}}$	Methods	Non-dimensional frequency coefficients				
		β_1	β_2	β_3	β_4	β_5
(a) located at $\xi_1 = x_1/L = 1.0$						
0.1	NAM	0.311053	3.173097	6.299059	9.435376	12.574323
	Gorman[10]	0.311050	3.173098	6.299058	9.435379	12.574318
1.0	NAM	0.860333	3.425618	6.437298	9.529334	12.645287
	Gorman[10]	0.860336	3.425617	6.437293	9.529336	12.645287
10.0	NAM	1.428870	4.305802	7.228110	10.200262	13.214185
	Gorman[10]	1.428871	4.305799	7.228112	10.200260	13.214186
(b) located at $\xi_1 = x_1/L = 0.5$						
0.1	NAM	0.432841	3.203935	6.314846	9.445948	12.582264
	Gorman[10]	0.432837	3.203938	6.314849	9.445946	12.582268
1.0	NAM	1.076874	3.643597	6.578333	9.629560	12.722299
	Gorman[10]	1.076869	3.643596	6.578332	9.629563	12.722300
10.0	NAM	1.496129	4.491480	7.495412	10.511670	13.541976
	Gorman[10]	1.496127	4.491478	7.495413	10.511674	13.541977

1.0 and the non-dimensional rotary inertia, $I^*_{0v} = 1.0$, the lowest five non-dimensional frequency coefficients β_j ($j = 1$–5) and the corresponding mode shapes of twisting angles $\bar{\theta}_j (j = 1$–5) were shown in Table 4 and Fig. 2, respectively. From Table 4 and Fig. 2 one sees that the lowest five

Table 4
The lowest five non-dimensional frequency coefficients β_j ($j = 1$–5) for a cantilever shaft carrying "two" concentrated elements (one rotary inertia and one torsional spring) at its free end

Concentrated elements	Methods	Non-dimensional frequency coefficients				
		β_1	β_2	β_3	β_4	β_5
$I_{01}^* = k_{R1}^* = 0.1$	NAM	0.326231	3.173128	6.299064	9.435378	12.574324
	Gorman[10]	0.326235	3.173127	6.299068	9.435379	12.574328
$I_{01}^* = k_{R1}^* = 1.0$	NAM	1.207793	3.448238	6.440954	9.530477	12.645779
	Gorman[10]	1.207797	3.448235	6.440956	9.530479	12.645775
$I_{01}^* = k_{R1}^* = 10.0$	NAM	2.841770	5.599018	8.228049	10.836159	13.580900
	Gorman[10]	2.841770	5.599022	8.228047	10.836163	13.580904

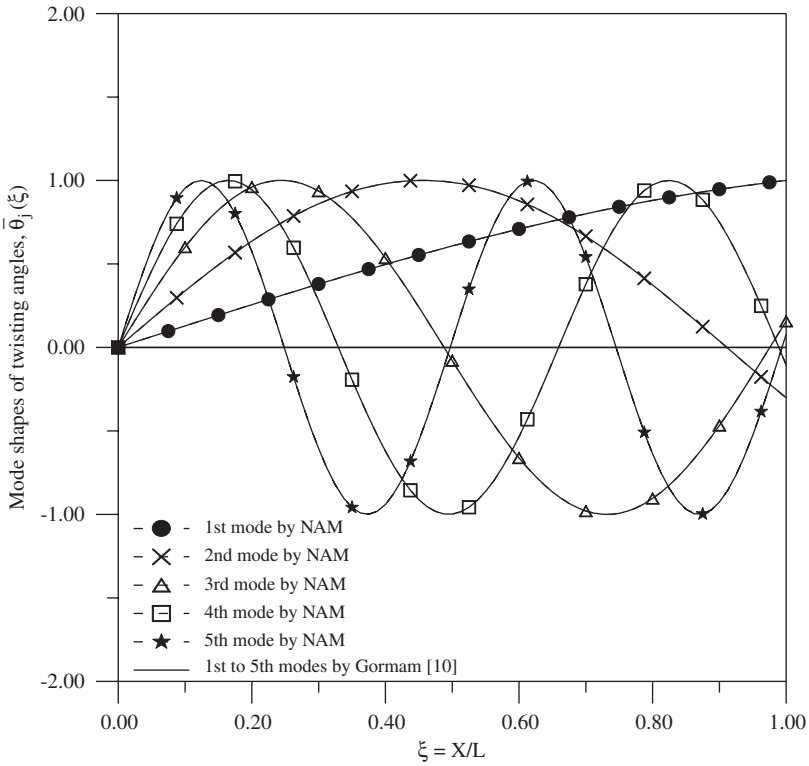

Fig. 2. The lowest five mode shapes of twisting angles, $\bar{\theta}_j(\xi)$ ($j = 1$–5), for the cantilever shaft carrying "two" concentrated elements (one rotary inertia and one torsional spring) at its free end with magnitudes of the non-dimensional torsional spring $k_{Rv}^* = 1.0$ and the non-dimensional rotary inertia $I_{0v}^* = 1.0$.

non-dimensional frequency coefficients and the corresponding mode shapes of twisting angles obtained from the NAM are in good agreement with those obtained from Gorman [10]. According to the above comparisons, it is believed that the NAM is an effective technique for the title problem.

Table 5
The locations and magnitudes of the three sets of concentrated attachments.

Sets of concentrated attachments	Locations of rotary inertia and/or torsional spring $\xi_j = x_j/L$					Magnitudes of torsional spring $k^*_{Rv} = k_{Rv}L/GI_p$					Magnitudes of rotary inertia $I^*_{0v} = \bar{J}_p L/I_{0v}$				
	ξ_1	ξ_2	ξ_3	ξ_4	ξ_5	k^*_{R1}	k^*_{R2}	k^*_{R3}	k^*_{R4}	k^*_{R5}	I^*_{01}	I^*_{02}	I^*_{03}	I^*_{04}	I^*_{05}
k^*_{Rv}	0.1	0.3	0.5	0.7	0.9	1.0	1.0	1.0	1.0	1.0					
I^*_{0v}	0.1	0.3	0.5	0.7	0.9						1.0	1.0	1.0	1.0	1.0
$k^*_{Rv} = I^*_{0v}$	0.1	0.3	0.5	0.7	0.9	1.0	1.0	1.0	1.0	1.0	1.0	1.0	1.0	1.0	1.0

Table 6
The lowest five natural frequencies for the shaft carrying five torsional springs with locations and magnitudes shown in Table 5

Boundary conditions	Methods	Natural frequencies (rad/s)				
		ω_1	ω_2	ω_3	ω_4	ω_5
CF	NAM	442.38625	847.76398	1328.39161	1825.68890	2328.35966
	FEM	442.32918	847.57916	1328.07013	1824.94767	2327.31655
		(0.0129%)	(0.0218%)	(0.0242%)	(0.0406%)	(0.0448%)
CC	NAM	625.96502	1084.57763	1575.94569	2076.75296	2607.94970
	FEM	625.85485	1084.38565	1575.66517	2076.31684	2607.38899
		(0.0176%)	(0.0177%)	(0.0178%)	(0.0210%)	(0.0215%)

Note: The percentage differences between $\omega_{j\mathrm{NAM}}$ and $\omega_{j\mathrm{FEM}}$ shown in the parentheses ( ) were determined with the formula: $\varepsilon_j = (\omega_{j\mathrm{NAM}} - \omega_{j\mathrm{FEM}}) \times 100\%/\omega_{j\mathrm{NAM}}$.

3.2. Free vibration analysis of the shaft carrying five torsional springs

Since the information regarding the exact natural frequencies and mode shapes of a uniform shaft carrying multiple concentrated elements has not been found yet, the numerical results of the current and the next subsections are compared with those obtained from the conventional FEM to confirm their reliability. For the CF and CC shafts carrying five torsional springs with locations and magnitudes shown in Table 5, the lowest five natural frequencies, ω_j ($j = 1$–5), were shown in Table 6 and the corresponding mode shapes of twisting angles, $\bar{\theta}_j (j = 1 - 5)$, were shown in Fig. 3. In the last figure, the dashed lines represent the mode shapes of twisting angles obtained from the present NAM and the solid lines represent those obtained from the conventional FEM. It is evident that they are in good agreement. For convenience of comparison, the free torsional vibration analysis of a uniform shaft without carrying any concentrated elements was also made by using NAM. Table 9 in Appendix B shows the lowest five natural frequencies, $\tilde{\omega}_j = (j = 1$–$5)$, with the CF and CC boundary conditions and Figs. 5(a)–(b) show the corresponding mode shapes of twisting angles. A comparison between Tables 9 and 6 reveals that the natural frequencies of the shaft "without" carrying any concentrated elements are smaller than the corresponding ones of the shafts carrying "five" torsional springs. The difference between ω_j and $\tilde{\omega}_j$, $\Delta\omega_j = \omega_j - \tilde{\omega}_j$,

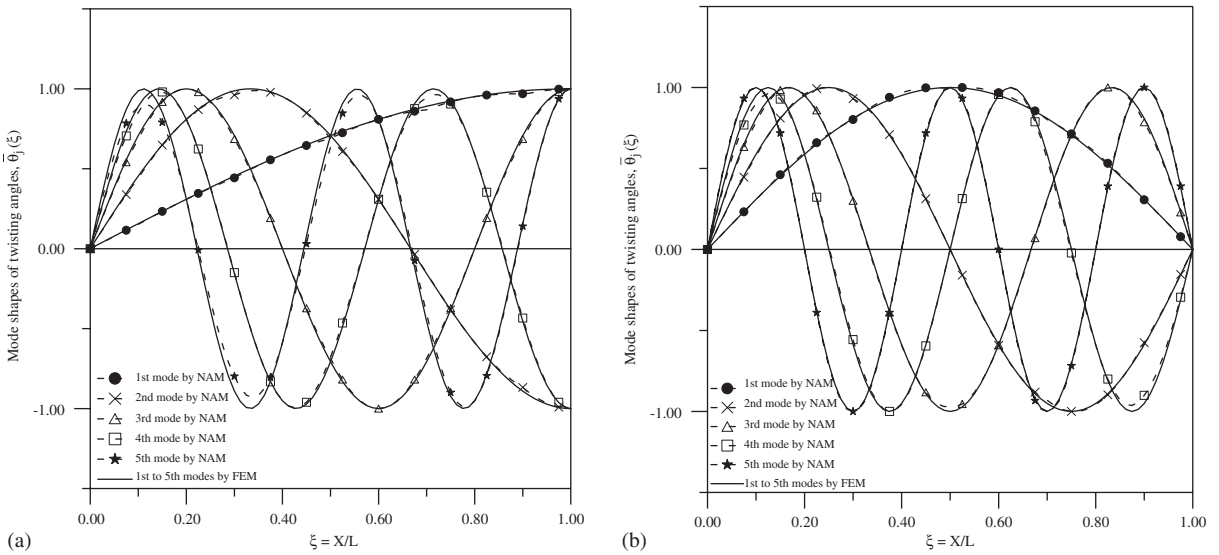

Fig. 3. The lowest five mode shapes of twisting angles, $\bar{\theta}_j(\xi)$ ($j = 1$–5), for the uniform shaft carrying five torsional springs with locations and magnitudes shown in Table 5 in the support conditions: (a) CF and (b) CC, obtained from the present numerical assembly method (NAM) and the conventional finite element method (FEM).

Table 7
The lowest five natural frequencies for the shaft carrying five rotary inertia with locations and magnitudes shown in Table 5

Boundary conditions	Methods	Natural frequencies (rad/s)				
		ω_1	ω_2	ω_3	ω_4	ω_5
CF	NAM	104.09671	304.98929	482.88004	619.40419	694.81096
	FEM	104.07651	304.92280	482.77525	619.19421	694.57263
		(0.0194%)	(0.0218%)	(0.0217%)	(0.0339%)	(0.0343%)
CC	NAM	206.38625	397.88841	557.56443	665.88763	704.63713
	FEM	206.36478	397.84384	557.43061	665.69385	704.36091
		(0.0104%)	(0.0112%)	(0.0240%)	(0.0291%)	(0.0392%)

decreases with the increasing mode number j. But the lowest five mode shapes of twisting angles of the shafts carrying "five" torsional springs shown in Fig. 3 look like those of the shaft "without" carrying any concentrated elements shown in Figs. 5(a)–(b). The five "identical" torsional springs "uniformly" distributed along the shaft length should be the main reason arriving at the last result.

The percentage differences between $\omega_{j\mathrm{NAM}}$ and $\omega_{j\mathrm{FEM}}$ shown in the parentheses ( ) of Table 6 were calculated with the formula: $\varepsilon_j = (\omega_{j\mathrm{NAM}} - \omega_{j\mathrm{FEM}}) \times 100\%/\omega_{j\mathrm{NAM}}$, where $\omega_{j\mathrm{NAM}}$ and $\omega_{j\mathrm{FEM}}$ denote the jth natural frequencies of the shafts carrying "five" torsional springs obtained from NAM and FEM, respectively. From Table 6 one finds that the maximum value of ε_j is $\varepsilon_5 = 0.0448\%$ (for the CF shaft), hence the accuracy of the NAM is good.

3.3. Free vibration analysis of the shaft carrying five rotary inertia

Instead of the torsional springs, for the same shaft carrying five rotary inertia with locations and magnitudes shown in Table 5, the lowest five natural frequencies, ω_j ($j = 1$–5), of the shaft were shown in Table 7. Comparing the results of Tables 7 and 9, one sees that the lowest five natural frequencies of the shaft carrying "five" rotary inertia, ω_j ($j = 1$–5), shown in Table 7 are smaller than the corresponding ones of the same shaft "without" carrying any concentrated elements, $\tilde{\omega}_j$ ($j = 1$–5), shown in Table 9. Besides, the maximum percentage difference between $\omega_{j\mathrm{NAM}}$ and $\omega_{j\mathrm{FEM}}$ shown in the parentheses ( ) of Table 7 is found to be $\varepsilon_5 = 0.0392\%$ (for the CC shaft). Since the corresponding mode shapes of twisting angles for the shafts carrying "five" rotary inertia are almost coincident with the ones for the shaft "without" carrying any concentrated elements (cf. Fig. 5), the former were not shown in this paper.

3.4. Free vibration analysis of the shaft carrying five torsional springs and five rotary inertia

Finally, the same shaft carrying five torsional springs and five rotary inertia is studied. For the case of "five" torsional springs and "five" rotary inertia with their locations and magnitudes as shown in Table 5, the lowest five natural frequencies of the shaft, ω_j ($j = 1$–5), were shown in Table 8. From Tables 8 and 9, it is seen that the lowest five natural frequencies of the shaft carrying "five" torsional springs and "five" rotary inertia are smaller than the corresponding ones of the shaft "without" carrying any concentrated elements. Besides, the maximum percentage difference between $\omega_{j\mathrm{NAM}}$ and $\omega_{j\mathrm{FEM}}$ shown in the parentheses ( ) of Table 8 is found to be $\varepsilon_5 = 0.0616\%$ (for the CC shaft). The corresponding mode shapes of twisting angles for the shaft carrying "five" torsional springs and those carrying "five" rotary inertia are also almost identical with the ones for the shaft "without" carrying any concentrated elements (cf. Fig. 5) and not shown here.

3.5. Influence of magnitude and location of the single torsional spring k_R

If $k_R^* = k_R L/GI_p$, then the influence of location of the single torsional spring k_R with magnitudes $k_R^* = 1.0$, $k_R^* = 5.0$ and $k_R^* = 10.0$, respectively, on the lowest three natural

Table 8
The lowest five natural frequencies for the shaft carrying five rotary inertia and five torsional springs with locations and magnitudes shown in Table 5

Boundary conditions	Methods	Natural frequencies (rad/s)				
		ω_1	ω_2	ω_3	ω_4	ω_5
CF	NAM	181.55200	339.90823	506.37430	638.56085	712.37468
	FEM	181.51496	339.83243	506.23302	638.34310	712.12891
		(0.0204%)	(0.0223%)	(0.0279%)	(0.0341%)	(0.0345%)
CC	NAM	254.69619	425.63206	578.40376	684.01115	722.02369
	FEM	254.66893	425.58353	578.26378	683.81141	721.57892
		(0.0107%)	(0.0114%)	(0.0242%)	(0.0292%)	(0.0616%)

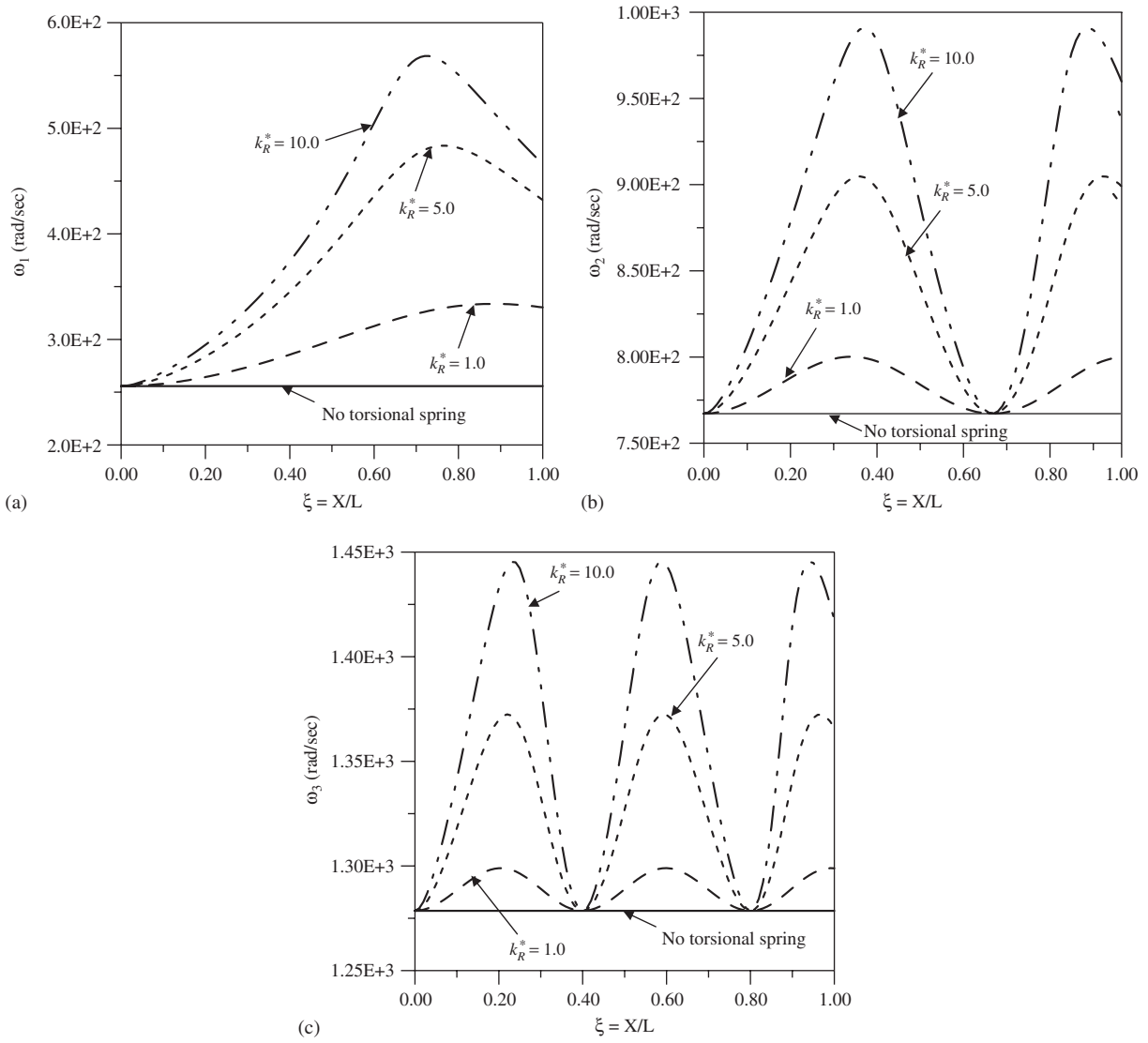

Fig. 4. Influence of magnitude and location of the single torsional spring on the lowest three natural frequencies of the cantilever shaft: (a) first natural frequency ω_1; (b) second natural frequency ω_2; and (c) third natural frequency ω_3.

frequencies of the cantilever shaft carrying a single "torsional spring" was shown in Figs. 4(a) for the first frequency ω_1, 4(b) for the second one ω_2 and 4(c) for the third one ω_3. From Fig. 4(a) one sees that the first natural frequency (ω_1) of the cantilever shaft increases when the distance between the single torsional spring k_R and the left clamped end of the shaft, x_R (or $\xi_R = x_R/L$, L is the shaft length), increases; for the non-dimensional torsional spring $k_R^* = 10.0$, the maximum frequency appears at the position $x_R \approx 0.74L$ instead of the position $x_R = 1.0L$ (at free end). From Figs. 4(b) and (c) one sees that, at any specified location of the single torsional spring k_R, the value

of ω_2 (or ω_3) also increases with increasing the magnitude of the single torsional spring k_R, but the influence of location of the single torsional spring on the second natural frequency ω_2 and the third one ω_3 is more complicated. From the second and third mode shapes of twisting angles of the cantilever shaft without carrying any concentrated elements shown in Fig. 5(a) one sees that there exists one node at $x \approx 0.675L$ in the second mode shape and two nodes at $x \approx 0.4L$ and $0.8L$, respectively, in the third mode shape. This will be the reason why the second natural frequency (ω_2) of the shaft carrying a single torsional spring for the case of $k_R^* = 1.0$ is equal to that with $k_R^* = 5.0$ or $k_R^* = 10.0$ when the torsional spring is located at $x_R \approx 0.675L$ (or $\xi_R = x_R/L \approx 0.675$) as one may see from Fig. 4(b). Similarly, when the torsional spring is located at node 1 with$x_{R1} \approx 0.4L$ or node 2 with $x_{R2} \approx 0.8L$, the influence of the magnitude of the torsional spring ($k_R^* = 1.0$, 5.0 or 10.0) on the third natural frequency (ω_3) of the shaft carrying a single torsional spring is nil as shown in Fig. 4(c). It is noted that the horizontal solid lines in Figs. 4(a)–(c) were used to indicate the first, second and third natural frequencies of the cantilever shaft without carrying any concentrated elements, respectively.

4. Conclusions

(1) For a uniform circular shaft carrying more than "two" concentrated elements, the exact natural frequencies and the corresponding mode shapes of twisting angles can be easily determined with the numerical assembly method (NAM). Comparing with the conventional finite element method (FEM), one of the main advantages of NAM is that the solutions of NAM are exact and those of FEM are approximate.
(2) If the total number of nodes for the rth mode shape is q and the distance between the ith node and the left supporting end of the cantilever shaft is denoted by x_{ci}, then the influence of magnitude of the torsional spring on the corresponding natural frequency ω_r is nil, when the torsional spring is located at $x = x_{ci}$ ($i = 1$–q) (i.e., located at any of the nodes).

Appendix A

For a uniform cantilever shaft carrying a set of concentrated elements (a rotary inertia together with a torsional spring) at $\xi_1 = x_1/L$, the "explicit" expression for the overall coefficient matrix $[B]_{(1)}$ was given by Eq. (A.1), while for that carrying two sets of concentrated elements at $\xi_1 = x_1/L$ and $\xi_2 = x_2/L$, its overall coefficient matrix $[B]_{(2)}$ was given by Eq. (A.2).

$$[B]_{(1)} = \begin{array}{c} \begin{matrix} \bar{C}_1 & \bar{C}_2 & \bar{C}_3 & \bar{C}_4 \end{matrix} \\ \begin{bmatrix} 0 & 1 & 0 & 0 \\ \sin(\beta\xi_1) & \cos(\beta\xi_1) & -\sin(\beta\xi_1) & -\cos(\beta\xi_1) \\ \nabla_{11} & \nabla_{21} & -\beta\cos(\beta\xi_1) & \beta\sin(\beta\xi_1) \\ 0 & 0 & \beta\cos\beta & -\beta\sin\beta \end{bmatrix} \end{array} \begin{matrix} 1 \\ 2 \\ 3 \\ 4 \end{matrix}, \tag{A.1}$$

$$[B]_{(2)} = \begin{array}{c} \begin{matrix} \bar{C}_1 & \bar{C}_2 & \bar{C}_3 & \bar{C}_4 & \bar{C}_5 & \bar{C}_6 \end{matrix} \\ \begin{bmatrix} 0 & 1 & 0 & 0 & 0 & 0 \\ \sin(\beta\xi_1) & \cos(\beta\xi_1) & -\sin(\beta\xi_1) & -\cos(\beta\xi_1) & 0 & 0 \\ \nabla_{11} & \nabla_{21} & -\beta\ \cos(\beta\xi_1) & \beta\ \sin(\beta\xi_1) & 0 & 0 \\ 0 & 0 & \sin(\beta\xi_2) & \cos(\beta\xi_2) & -\sin(\beta\xi_2) & -\cos(\beta\xi_2) \\ 0 & 0 & \nabla_{12} & \nabla_{22} & -\beta\ \cos(\beta\xi_2) & \beta\ \sin(\beta\xi_2) \\ 0 & 0 & 0 & 0 & \beta\ \cos\beta & -\beta\ \sin\beta \end{bmatrix} \end{array} \begin{matrix} 1 \\ 2 \\ 3 \\ 4 \\ 5 \\ 6 \end{matrix}, \quad \text{(A.2)}$$

where

$$\nabla_{11} = \beta\ \cos(\beta\xi_1) - \frac{\beta^2}{I_{01}^*}\sin(\beta\xi_1) + k_{R1}^*\ \sin(\beta\xi_1),$$

$$\nabla_{21} = -\beta\ \sin(\beta\xi_1) - \frac{\beta^2}{I_{01}^*}\cos(\beta\xi_1) + k_{R1}^*\ \sin(\beta\xi_1),$$

$$\nabla_{12} = \beta\ \cos(\beta\xi_2) - \frac{\beta^2}{I_{02}^*}\sin(\beta\xi_2) + k_{R2}^*\ \sin(\beta\xi_2),$$

$$\nabla_{22} = -\beta\ \sin(\beta\xi_2) - \frac{\beta^2}{I_{02}^*}\cos(\beta\xi_2) + k_{R2}^*\ \sin(\beta\xi_2).$$

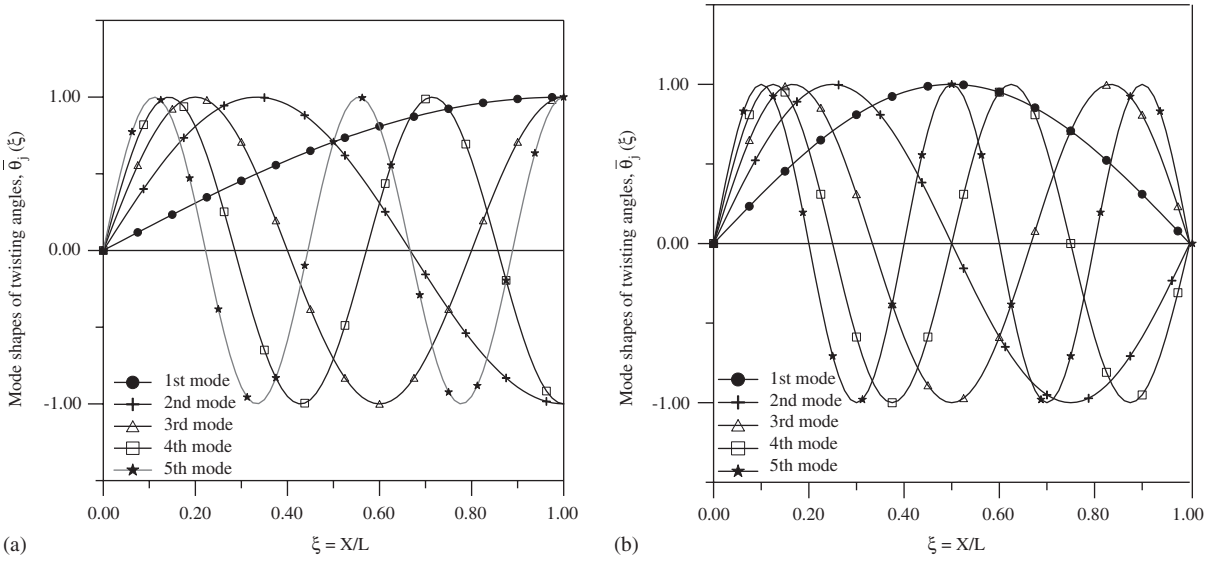

Fig. 5. The lowest five mode shapes of twisting angles, $\bar{\theta}_j(\xi)$ ($j = 1$–5), for the shaft without carrying any concentrated elements in the support conditions: (a) CF and (b) CC, obtained from NAM.

Table 9
The lowest five natural frequencies, $\tilde{\omega}_j$ ($j = 1$–5), for the shaft without carrying any concentrated elements obtained from NAM

Boundary Conditions	Natural frequencies (rad/sec)				
	$\tilde{\omega}_1$	$\tilde{\omega}_2$	$\tilde{\omega}_3$	$\tilde{\omega}_4$	$\tilde{\omega}_5$
CF	255.71565	767.14691	1278.57825	1790.00961	2301.44075
CC	511.43130	1022.86258	1534.29394	2045.72518	2557.15652

Appendix B

The lowest five natural frequencies $\tilde{\omega}_j$ ($j = 1$–5) and the corresponding mode shapes of twisting angles, $\bar{\theta}_j(\xi)$ ($j = 1$–5), for the shaft without carrying any concentrated elements in the CF and CC boundary conditions were shown in Table 9 and Figs. 5(a)–(b), respectively.

References

[1] H. Holzer, *Analysis of Torsional Vibration*, Springer, Berlin, 1921.
[2] W.K. Wilson, *Practical Solution of Torsional vibration Problems*, third ed., vols. 1 & 2, Chapman & Hall, London, 1956, 1963.
[3] A.H. Church, *Mechanical Vibration*, Wiley, New York, 1957.
[4] T.W. Spaetgens, B.C. Vancouver, Holzer method for force-damped torsional vibrations, *Journal of Applied Mechanics* 17 (1950) 59–63.
[5] J.P. Den Hartog, J.P. Li, Forced torsional vibrations with damping: an extension of Holzer's method, *Journal of Applied Mechanics, Transactions of ASME* 68 (1946) 276–280.
[6] J.S. Wu, W.H. Chen, Computer method for forced torsional vibration of propulsive shafting system of marine engine with or without damping, *Journal of Ship Research* 26 (1982) 176–189.
[7] L. Meirovitch, *Analytical Methods in Vibrations*, MacMillan, New York, 1967.
[8] S. Doughty, G. Vafaee, Transfer matrix eigensolutions for damped torsional systems, *Transactions of ASME, Journal of Vibration, Acoustics, Stress and Reliability in Design* 107 (1985) 128–132.
[9] J.S. Wu, I.H. Yang, Computer method for torsion-and-flexure-coupled forced vibration of shafting system with damping, *Journal of Sound and Vibration* 180 (1995) 417–435.
[10] D.J. Gorman, *Free Vibration Analysis of Beams and Shafts*, Wiley, New York, 1975.
[11] R.D. Blevins, *Formulas for natural frequency and mode shape*, Van Nostrand, New York, 1979.
[12] C.K. Rao, Torsional frequencies and mode shapes of generally constrained shafts and piping, *Journal of Sound and Vibration* 125 (1) (1988) 115–121.
[13] J.S. Wu, H.M. Chou, A new approach for determining the natural frequencies and mode shapes of a uniform beam carrying any number of sprung masses, *Journal of Sound and Vibration* 220 (3) (1999) 451–468.
[14] J.S. Wu, D.W. Chen, Free vibration analysis of a Timoshenko beam carrying multiple spring-mass systems by using the numerical assembly technique, *International Journal for Numerical Methods in Engineering* 50 (2001) 1039–1058.
[15] D.W. Chen, J.S. Wu, The exact solutions for the natural frequencies and mode shapes of non-uniform beams carrying multiple spring–mass systems, *Journal of Sound and Vibration* 255 (2) (2002) 299–322.
[16] J.D. Faires, R.L. Burden, *Numerical Methods, PWS Publishing Company*, Boston, USA, 1993.